



FY-3D and FY-3C onboard observations for differential code biases estimation

Xingxing Li^{1,2} · Tengzhou Ma¹ · Weiliang Xie² · Keke Zhang¹ · Jiaxin Huang¹ · Xiaodong Ren¹

Received: 26 August 2018 / Accepted: 26 March 2019 / Published online: 3 April 2019
© Springer-Verlag GmbH Germany, part of Springer Nature 2019

Abstract

With the development of Low Earth Orbit satellites, differential code biases (DCBs) estimation based on onboard observations has been widely studied. In this study, onboard observations of BDS and GPS satellites by the Chinese Fengyun-3D (FY-3D) and Fengyun-3C (FY-3C) satellites are applied to estimate BDS and GPS DCBs. Since only the code observations of C1C and C2W for GPS, and C2I and C7I for BDS are tracked by FY-3D and FY-3C, the DCB types of GPS C1C-C2W and BDS C2I-C7I are estimated with code multipath considered. First, the DCB estimates based on FY-3D onboard observations are analyzed. When jointly processing BDS + GPS onboard observations, the stability of satellite and receiver DCBs for both BDS and GPS has better consistency with the DCB products of the German Aerospace Center (DLR) and the Chinese Academy of Science than that for the single-system solutions (BDS-only solution and GPS-only solution). This is reasonable because more onboard observations are used in BDS + GPS solution, which can improve the strength of the DCB estimation. The variations of receiver DCB are analyzed as a function of geomagnetism and solar activity, but little relationship between them has been found. Compared with the FY-3C solution, the FY-3D solution can achieve a more stable satellite DCB with a stability improvement of 33%, 48%, 62% and 56% for GPS, BDS GEO, IGSO, and MEO satellites, respectively. Meanwhile, the receiver DCB of FY-3D is more stable than that of FY-3C as well. These improvements of satellite and receiver DCBs can be due to the enhancement of FY-3D GNSS Occultation Sounder (GNOS) instrument, which provides more observations with higher quality. Furthermore, both FY-3D and FY-3C onboard observations are processed together to estimate BDS and GPS DCBs. Compared with the FY-3D solution, the stability of satellite DCB can be improved by 16%, 9% and 7% for GPS, BDS GEO and IGSO satellites DCB, respectively, when both FY-3D and FY-3C onboard observations are jointly processed. The impact of DCB estimation on estimating the vertical total electron content (VTEC) is also investigated. Compared with FY-3D GPS-only and BDS + GPS solutions, the VTEC estimates along the FY-3D orbit can achieve more realistic results for FY-3D + FY-3C solution.

Keywords BDS · GPS · Low Earth Orbit satellite · FY-3D · FY-3C · Differential code bias

Introduction

Code bias physically corresponds to a time delay due to signal propagation through the hardware, such as the antenna and different analog components. Differential code biases (DCBs) are code biases between two different frequencies or signal structures which exist in the Global Navigation

Satellite System (GNSS). They are important for precise applications, such as precise point positioning and ionosphere monitoring (Schaer 1999; Li et al. 2018a). Although DCBs can be determined within an anechoic chamber, they can be affected by hardware aging, temperature, and other factors (Sanz et al. 2017). Thus, DCBs should be re-determined during the service period of GNSS.

Generally, DCBs can be estimated by the dual-frequency geometry-free (GF) combination of ground-based observations (Montenbruck et al. 2014; Li et al. 2018b). There are two main ways to estimate DCBs: the first method is estimating DCBs together with regional or global ionosphere maps (Schaer 1999; Mannucci et al. 1998; Hernandez-Pajares et al. 1999). A well-known application for this method is the

✉ Xingxing Li
lxlq109121@gmail.com

¹ School of Geodesy and Geomatics, Wuhan University, 129 Luoyu Road, Wuhan 430079, Hubei, China

² German Research Centre for Geosciences (GFZ), 14473 Telegrafenberg, Potsdam, Germany

product of Global Ionosphere Maps (GIM) and the related DCBs provided by the International GNSS Service (IGS) since 1998. Another application for this method is the product of multi-GNSS DCBs provided by the Chinese Academy of Science (CAS) which locally models the ionosphere above each station of the network (Wang et al. 2016). This kind of DCB product can be obtained at <ftp://ftp.gipp.org.cn/project/dcb/mgexdcb/>. The second method is using the prior knowledge of the ionosphere and eliminating the ionospheric delay from the GF combination. This method is adopted by the German Aerospace Center (DLR) (Montenbruck et al. 2014). The corresponding DCB product is available at <ftp://cddis.gsfc.nasa.gov/pub/gps/products/mgex/dcb/>.

Since most Low Earth Orbit (LEO) satellites are equipped with GNSS receivers, new methods of DCB estimation based on onboard observations have been proposed. Most studies use the product of GPS satellite DCBs to derive the vertical total electron content (VTEC) and onboard receiver DCB (Yue et al. 2011; Zakharenkova and Cherniak 2015). Lin et al. (2016) and Zhong et al. (2016a) treated both satellite and onboard receiver DCBs as unknown parameters and estimated them sequentially. Wautelet et al. (2017) simultaneously estimated VTEC, satellite and onboard receiver DCBs in a least-square adjustment.

The FY-3 series of satellites are the Chinese second-generation polar-orbiting meteorological satellites. The FY-3C satellite is the first operational satellite of the FY-3 series orbiting at an altitude of 836 km and was launched on September 23, 2013. Li et al. (2017b) have estimated and analyzed DCBs based on FY-3C onboard observations. The FY-3D satellite is the second operational satellite of FY-3 series of satellites, which is also at an altitude of 836 km and was launched on November 15, 2017. Both FY-3D and FY-3C carry a GNSS Occultation Sounder (GNOS) instrument, which can simultaneously track dual-frequency pseudorange and phase observations of BDS and GPS (Bai et al. 2014). However, compared to the GNOS of FY-3C, there are three types of enhancements for the GNOS of FY-3D: (1) change of the occultation antenna type. One extra antenna patch has been added to the atmospheric occultation antenna, which allows the GNOS to receive the occultation signals from a wider azimuth range with better quality. (2) More channels for positioning and occultation. The number of dual-frequency channels GPS and BDS of FY-3D GNOS has been increased to 17 and 12, respectively, which can ensure more stable and accurate precise orbit determination (POD) results and more occultation events. (3) The FY-3D GNOS provides L2C and B1I open-loop (OL) tracking, which can secure more robust tracking capacity (Cai et al. 2017).

With the enhanced GNOS, the FY-3D satellite can track more good-quality BDS and GPS observations compared to FY-3C; one should expect more accurate estimates for BDS and GPS DCBs. Also, since FY-3D and FY-3C can

track dual-system observations, the onboard observations can make an even better contribution for GNSS DCB estimation, especially for BDS.

First, we describe the data and methodology, considering also code multipath. Next, the estimated BDS and GPS DCBs are analyzed and discussed for different solutions such as GPS-only, BDS + GPS and FY3D + FY3C. In addition, several factors which may affect the DCB estimation with these LEO satellites, such as geomagnetism and solar activity, are also analyzed and discussed in detail. Also, the impact of DCB estimation on TEC estimation is investigated. Finally, conclusions are presented.

Data and methodology

In this study, BDS and GPS onboard observations in 30-second interval from FY-3D and FY-3C for the time DOY 356, 2017 to DOY 019, 2018 are used to estimate BDS and GPS DCBs. Since only code observations of C1C and C2W for GPS, and C2I and C7I for BDS are tracked by FY-3D and FY-3C, the DCB types of GPS C1C-C2W and BDS C2I-C7I are estimated. The cutoff elevation mask of 30° is set to reduce the mapping function errors. In addition, carrier phase smoothed pseudorange is used to improve the precision of DCB estimation. The onboard observations of pseudorange and carrier phase can be expressed as:

$$\begin{cases} P_{r,i}^s = \rho_r^s + \frac{40.3}{f_i^2} \cdot \text{STEC} + c \cdot (dt_r - dt^s) + b_{r,i} + b^{s,i} + \text{MP}_i + \delta_i \\ L_{r,i}^s = \rho_r^s - \frac{40.3}{f_i^2} \cdot \text{STEC} + c \cdot (dt_r - dt^s) + B_{r,i}^s + \Delta\varphi_{r,i}^s + \varepsilon_i \end{cases} \quad (1)$$

where the superscript s represents the GNSS satellite, the subscript r and i refer to receiver and frequency, respectively; $P_{r,i}^s$ and $L_{r,i}^s$ represent the pseudorange and carrier phase observations in meter at f_i ($i = 1, 2$), respectively; ρ_r^s is the geometric distance from LEO satellite to GPS or BDS satellite; STEC is the slant total electron content in the unit of TECU; dt_r and dt^s refer to receiver and satellite clock offsets, respectively; c is the light speed in vacuum; $b_{r,i}$ and $b^{s,i}$ stand for code biases for receiver and satellite at f_i , respectively; $B_{r,i}^s$ is the phase ambiguity in meter, and $\Delta\varphi_{r,i}^s$ is the phase wind-up error. MP_i is the multipath error of pseudorange. δ_i and ε_i are the measurement noises of pseudorange and carrier phase, respectively.

In the estimation of space-calibrated DCB, there are two important procedures for data processing: (1) the cycle slip and outlier detection. In this study, the cycle slip and outlier are detected based on the TurboEdit algorithm proposed by Blewitt (1990). (2) The elimination of code multipath. Since the space-calibrated DCBs are associated with multipath modeling of the LEO satellite, which mainly affects the quality of the observation of carrier phase smoothed

pseudorange, the code multipath error should be eliminated before smoothing (Yue et al. 2011; Li et al. 2017b). The code multipath error can be calculated by multipath combination as used in Montenbruck and Kroes (2003). Figures 1 and 2 show the GPS and BDS multipath maps in terms of elevation and azimuth of FY-3C and FY-3D. Note that the elevation

and azimuth are calculated in the antenna reference frame (ARF), which is described in Li et al. (2017a). MP1 refers to the multipath error of GPS C1C or BDS C2I, and MP2 refers to the multipath error of GPS C2W or BDS C7I.

As shown in Fig. 1, the GPS MP1 is mainly concentrated in the area with elevation less than 30° and the fore hemisphere.

Fig. 1 GPS and BDS multipath maps (unit: m) based on FY-3C onboard observations with grid solution of 2° × 2°

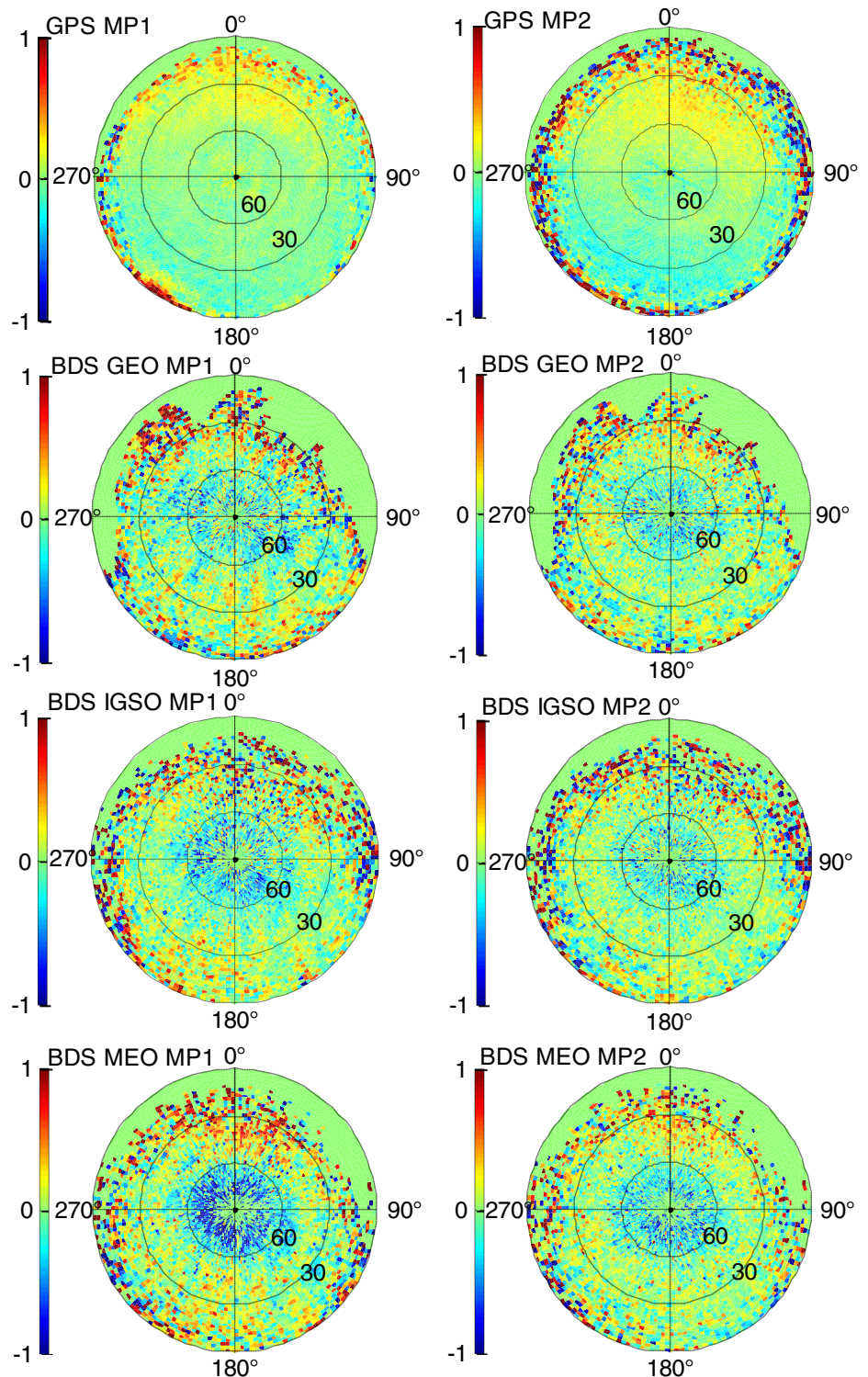
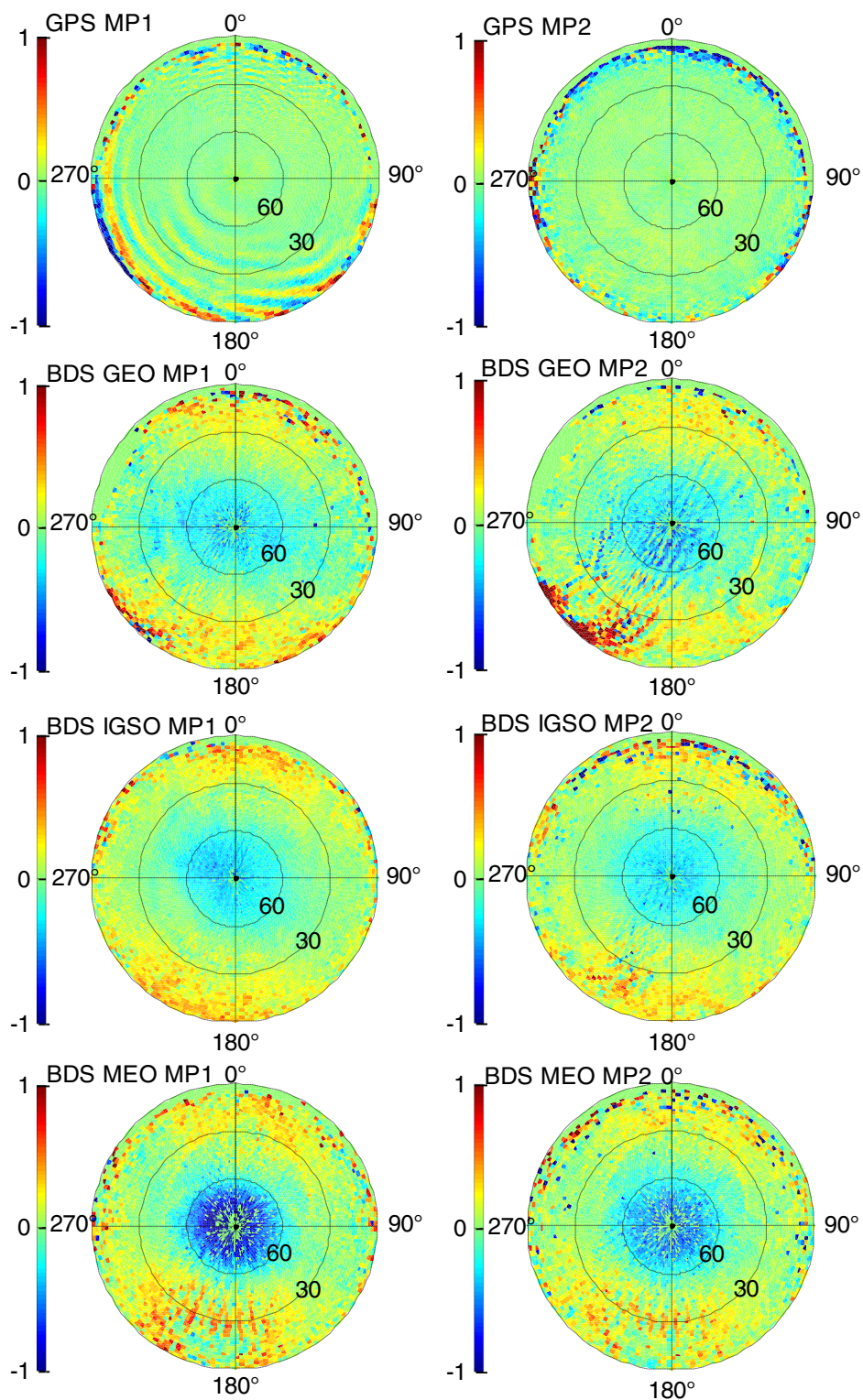


Fig. 2 GPS and BDS multipath maps (unit: m) based on FY-3D onboard observations with grid solution of $2^\circ \times 2^\circ$



The GPS MP2 also shows such phenomenon, but the multipath error can generally reach 1 m when elevation is less than 30° . Such system bias comes from the superposition of the direct signal with interfering signals using a different signal path. As for a spaceborne GNSS receiver, they are closely

associated with signal reflections caused by the surface of the LEO satellite (Montenbruck and Kroes 2003). For BDS GEO, IGSO and MEO MP1, there are systematic biases for elevation larger than 60° , which are about -0.3 m for BDS GEO and IGSO, -0.6 m for BDS MEO. The negative system bias found

in the BDS signals is not detected in the GPS signals. Such bias may be caused by the BDS spacecraft internal multipath (Montenbruck et al. 2013). Also, the MP1 value can reach 1 m in low elevation area. The MP2 of BDS GEO, IGSO and MEO shows similar patterns as MP1, but with smaller values when for elevation larger than 60°, especially for MEO MP2. Obviously, the maps of BDS GEO, IGSO and MEO contain both code multipath errors and BDS satellite-induced code pseudorange variations.

In Fig. 2, it can be seen that FY-3D has different patterns of the multipath errors compared with FY-3C. For GPS, the MP1 and MP2 are sparsely distributed in whole map. There is almost no multipath in areas where the elevation is larger than 30°, especially for MP2. For BDS GEO, IGSO and MEO MP1, there are also systematic biases when the elevation is larger than 60°. Such phenomena have also been found in BDS GEO, IGSO and MEO MP2. The MEO MP2 is less than MEO MP1 when elevation is larger than 60°. In addition, the MP1 and MP2 of BDS GEO, IGSO and MEO of FY-3D in low elevation area are quite smaller than that of FY-3C. Comparatively, the difference of multipath error between FY-3C and FY-3D proves that the FY-3D GNOS has adopted a better multipath mitigation technique.

After applying the BDS and GPS multipath maps correction, the residual errors of pseudorange are assumed to have a zero-mean average over the data arc. The GF combination for pseudorange and carrier phase can be obtained by differencing observations between two frequencies, which can be written as:

$$\begin{cases} P_{r,4}^s = P_{r,1}^s - P_{r,2}^s = \alpha \cdot \text{STEC} + \text{DCB}_r + \text{DCB}^s \\ L_{r,4}^s = L_{r,1}^s - L_{r,2}^s = -\alpha \cdot \text{STEC} + B_{r,12}^s + \Delta\varphi_{r,12}^s \end{cases} \quad (2)$$

where α is the factor of $40.3 \cdot (f_2^2 - f_1^2) / (f_2^2 \cdot f_1^2)$; DCB_r and DCB^s are the DCB of receiver and satellite between f_1 and f_2 , respectively; The phase wind-up can be effectively corrected with a nominal attitude for the orbital day time. However, during the orbit eclipse, satellites usually suffer from the yaw rate maximum to ensure the solar maximum radiation. This may lead to errors when we use nominal attitude model to compute phase wind-up correction. For FY-3 series satellites, a strict attitude control regime with a three-axis stabilization is employed in the satellite platform, which means that the mis-modeling errors of the LEO altitude are very small (Yang et al. 2012). Also, the errors of GNSS and LEO altitude model during the eclipse can be effectively weakened in the smoothing process. Hence, the mis-modeling errors of GNSS and LEO altitude can be neglected in the DCB estimation processing. After the smoothing process, the observation of carrier phase smoothed pseudorange can be described as (Montenbruck et al. 2014)

$$L_{\text{sm}} = \alpha \cdot \text{STEC} + \text{DCB}_r + \text{DCB}^s \quad (3)$$

where L_{sm} is the observation of carrier phase smoothed pseudorange. As indicated in some studies, the F&K geometric mapping function proposed by Foelsche and Kirchengast (2002) can be used for the LEO-based methods to convert the STEC to the VTEC when the assumption of spherical symmetry is adopted (Yue et al. 2011; Zhong et al. 2016b). Under the assumption of spherical symmetry, the VTECs of each receiver-satellite pair at one epoch are set to the same value. The relationship between STEC and VTEC can be expressed as:

$$\begin{aligned} \text{STEC} &= F\&Kmf \cdot \text{VTEC} \\ &= \frac{1 + (h_{\text{shell}} + R_e) / (H_{\text{LEO}} + R_e)}{\cos z + \sqrt{(h_{\text{shell}} + R_e)^2 / (H_{\text{LEO}} + R_e)^2 - \sin^2 z}} \cdot \text{VTEC} \end{aligned} \quad (4)$$

where z is the elevation angle of satellite observed from the spacecraft; R_e represents the earth radius; h_{shell} and H_{LEO} refer to the plasmasphere effective height (PEH) and the altitude of spacecraft orbit. Zhong et al. (2016b) evaluated the performance of the F&K mapping function at different PEHs and found a centroid method based on $F_{10.7}$ (Solar Radio Flux at 10.7 cm) is more applicable for onboard DCB and VTEC estimation. The centroid method can be expressed as:

$$h_{\text{shell}} = (0.0027 \cdot F_{10.7} + 1.79) \cdot H_{\text{LEO}} - 5.52 \cdot F_{10.7} + 1350 \quad (5)$$

After applying (4) and (5) to (3), the estimated parameters are VTEC, DCB_r and DCB^s . For a given observation epoch, if one onboard receiver observes n GPS and r BDS satellites simultaneously, the observation model can be written as:

$$\begin{bmatrix} L_{\text{sm}}^1 \\ L_{\text{sm}}^2 \\ \vdots \\ L_{\text{sm}}^n \\ L_{\text{sm}}^{n+1} \\ \vdots \\ L_{\text{sm}}^{n+r} \end{bmatrix} = \begin{bmatrix} \alpha \cdot mf^1 & 1 & 0 & \dots & \dots & 1 & 0 \\ \alpha \cdot mf^2 & 0 & 1 & \dots & \dots & 1 & 0 \\ \vdots & & \vdots & & & & \\ \alpha \cdot mf^n & 0 & 0 & \dots & \dots & 1 & 0 \\ \alpha \cdot mf^{n+1} & 0 & 0 & \dots & \dots & 0 & 1 \\ \vdots & & \vdots & & & & \\ \alpha \cdot mf^{n+r} & 0 & 0 & \dots & \dots & 1 & 0 & 1 \end{bmatrix} \cdot \begin{bmatrix} \text{VTEC} \\ \text{DCB}^1 \\ \text{DCB}^2 \\ \vdots \\ \text{DCB}^{n+r} \\ \text{DCB}_{\text{GPS}} \\ \text{DCB}_{\text{BDS}} \end{bmatrix} \quad (6)$$

where mf^i is the coefficient of VTEC calculated by (4) referred to satellite i . For a given observation epoch, equation (6) is not solvable. But in a given day, the VTEC parameters are solved by each epoch, considering the DCB parameters of GNSS satellite and receiver to be constant during a day. Thus, the DCBs and VTEC can be de-correlated and all parameters can be estimated simultaneously in a least-square adjustment. Note that a zero-mean condition for all satellite DCBs should be imposed to separate satellite and receiver DCBs. The zero-mean condition can be denoted as:

$$\sum_{s=1}^{N^G} \text{DCB}^s = 0, \quad \sum_{s=1}^{N^B} \text{DCB}^s = 0 \quad (7)$$

where N^G and N^B refer to the total number of GPS and BDS satellites, respectively.

Results, analysis and discussion

We first analyze the performance of DCB estimation with FY-3D onboard observations. As the LEO DCB estimation may be affected by the space environment, the impact of geomagnetism and solar activity on LEO DCB estimation is discussed subsequently. After that, we briefly make a comparison with DCB estimation between FY-3D and FY-3C, FY-3D-only and FY-3D + FY-3C. We finally discuss the impact of DCB estimation on the estimation of TEC.

DCB estimation with FY-3D onboard observations

In this part, three solutions, namely BDS-only, GPS-only and BDS + GPS, are performed to evaluate the performance of DCB estimation with BDS and GPS onboard observations from FY-3D. The results are assessed from the following two aspects: (1) the monthly mean difference between FY-3D solutions and DCB products of DLR and CAS. (2) The standard deviation (STD) values of the daily DCB. The STD is also defined as monthly stability. The smaller the STD, the higher the stability. It is worth noting that the time series of daily DCB values of DCB products and our results presents jumps and drifts for the entire period of study. Before comparing different DCB solutions, the time series of daily DCB values should be realigned by using a fixed common set of satellites throughout the period of interest (Sanz et al. 2017).

Estimating GPS DCBs

The monthly mean differences of GPS satellite DCBs between FY-3D solutions and DCB products are given in Fig. 3. Note that G04 DCB is not estimated due to lack of observations. For both GPS-only and BDS + GPS solutions, their monthly mean differences with DCB products are within ± 1 ns. This value is consistent with a previous study by Wautelet et al. (2017), who only used dual pseudorange onboard observations from Jason-2 which is at the altitude of 1336 km. Although smoothed observations of higher precision are used in this contribution, the onboard observations from FY-3D are easier to be affected by the plasmasphere due to the relative lower orbit than the Jason-2 observations. For GPS-only and BDS + GPS solutions, their means of the absolute difference with respect to the DLR product are 0.321 and 0.322 ns, and the values with respect to the CAS product are 0.321 and 0.323 ns, respectively. It can be concluded that monthly means of GPS satellite

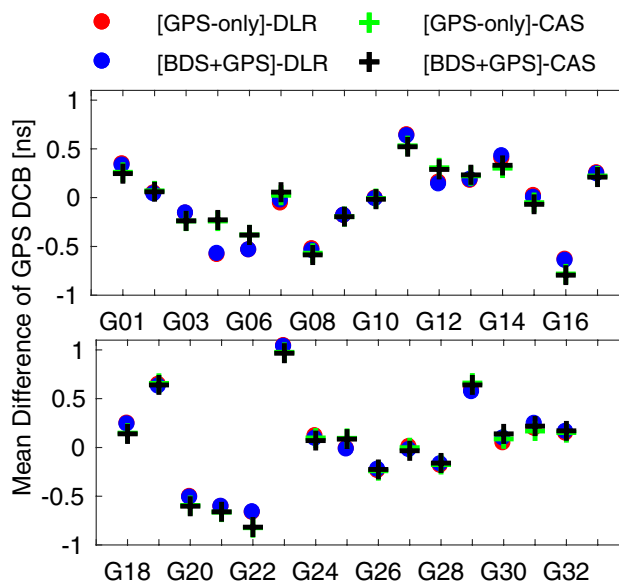


Fig. 3 Monthly mean differences of GPS satellite DCBs between FY-3D solutions and DCB products of DLR and CAS. Different symbols represent different situations

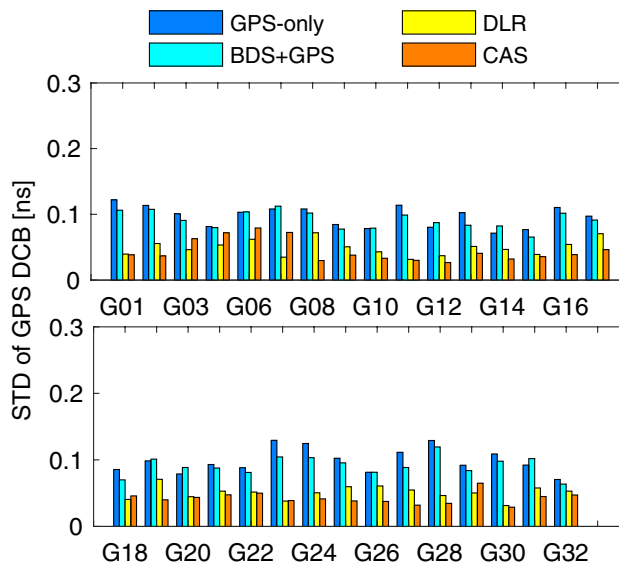


Fig. 4 Monthly STDs of GPS satellite DCBs. Different symbols represent different solutions. The DLR and CAS products are shown as references

DCBs for both GPS-only and BDS + GPS solutions are at the same level.

In Fig. 4, the monthly STDs of GPS satellite DCBs are shown. The STD values of both DLR and CAS products are less than 0.1 ns, and STDs of GPS-only and BDS + GPS solutions fluctuate around 0.1 ns. The mean STDs of GPS satellite DCBs for GPS-only, BDS + GPS, DLR and CAS

solutions are 0.098, 0.092, 0.050 and 0.044 ns, respectively. Compared with the GPS-only solution, the monthly stability of satellite DCBs for BDS + GPS solution could be improved overall by 6%. Note that the mean STD based on the FY-3D solutions is about twice that of the DLR and CAS products. This is reasonable because that the DCB products of DLR and CAS are estimated by hundreds of ground stations which can achieve better stability. Also, because of the rapid movement of the LEO satellite, which is about 7 km/s, the tracking arcs between the LEO satellite and GNSS satellites are quite short. Within such a short arc, the ambiguity cannot be effectively converged, as compared to the ground-based calibration, which results in the poorer stability for space-based calibration.

The time series of the FY-3D receiver DCB for GPS is illustrated in Fig. 5. The receiver DCBs for GPS-only and BDS + GPS solutions share similar trends in the time series and vary within 1 ns. Their monthly mean and STD are -17.637 ± 0.166 ns and -17.600 ± 0.131 ns, respectively. The receiver DCB of GPS for the BDS + GPS solution is more stable than that for GPS-only solution, with a stability improvement of 21%. It is noteworthy that there is a periodic variation of about 6 days in the FY-3D receiver DCB for GPS. The similar phenomenon can also be found in the result of the FY-3C receiver DCB. For FY-3C and FY-3D receivers, the nominal orbital regression period is about 5.5 days. The periodic phenomenon may be closely related to the orbital regression period of FY-3 satellites.

Estimating BDS DCBs

Figure 6 shows the monthly mean differences of BDS satellite DCBs between FY-3D solutions and DCB products. For both BDS-only and BDS + GPS solutions, their monthly mean differences with DCB products are within ± 1.5 ns. Compared with BDS-only solution, the means of the absolute difference with respect to DLR and CAS products are slightly reduced from 0.446 to 0.414 ns and from 0.513 to 0.480 ns, respectively, when using BDS + GPS solution. The monthly mean of BDS satellite DCBs for the BDS + GPS

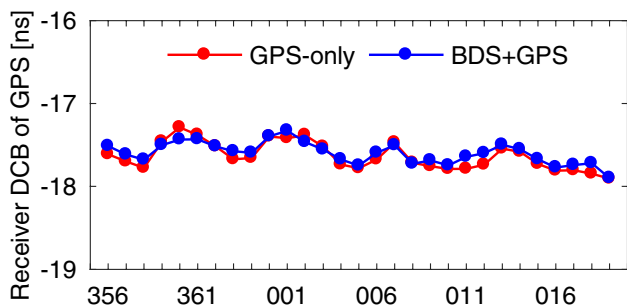


Fig. 5 Time series of FY-3D receiver DCB for GPS of 29 days

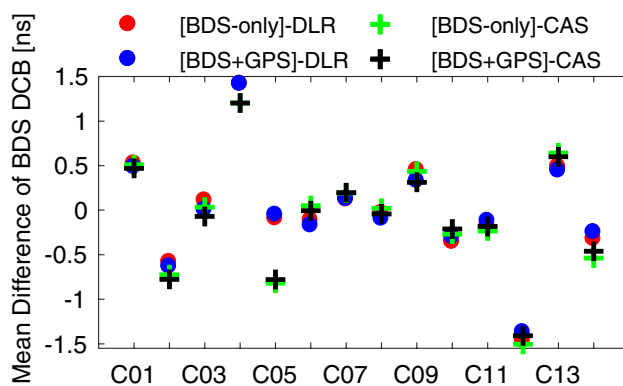


Fig. 6 Monthly mean differences of BDS satellite DCBs between FY-3D solutions and DCB products

solution has better consistency with the products of DLR and CAS.

The monthly STDs of BDS satellite DCBs are illustrated in Fig. 7. As can be seen, different kinds of BDS satellites show different scales of STD. The GEO satellites have the largest STDs, followed by IGSO and MEO satellites. This is related to the stationary characteristics and regional coverage of BDS GEO satellites, which results in less onboard GEO observations. In general, the STD of the BDS-only and BDS + GPS solutions is less than 0.2 ns. The means of monthly STD for BDS satellite DCBs are given in Table 1. Due to the special design of the BDS constellation, the BDS satellites are grouped into GEO, IGSO, MEO satellites and their statistics are calculated separately. The means of monthly STD for FY-3D solutions are generally larger than that of DLR and CAS products, except that of MEO satellites for BDS + GPS solution. Compared with BDS-only solution, the mean STDs of BDS satellites for BDS + GPS solution can be improved by 9%, 26% and 34% for BDS GEO, IGSO and MEO satellites, respectively.

The time series of FY-3D receiver DCB for BDS is illustrated in Fig. 8. The monthly mean and STD of FY-3D receiver DCB for both BDS-only and BDS + GPS solutions

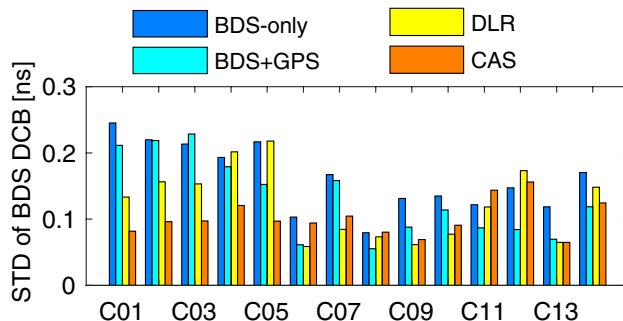
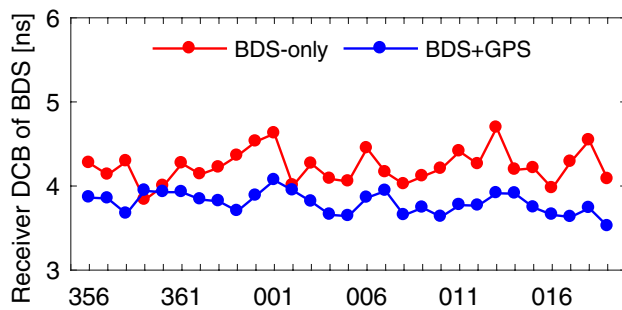


Fig. 7 Monthly STDs of BDS satellite DCBs

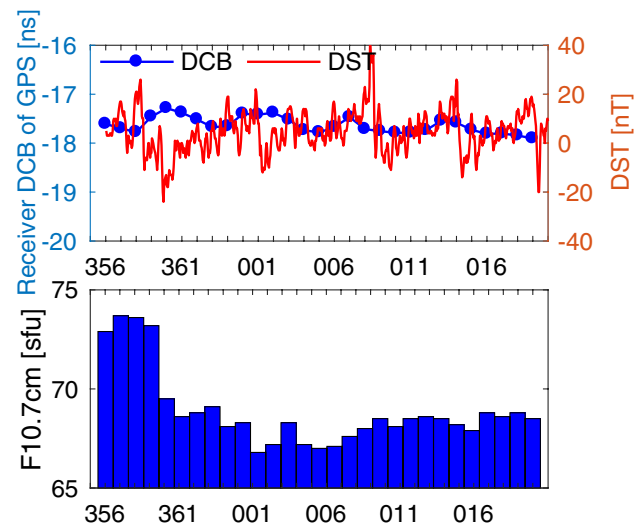
Table 1 Statistics of mean values of monthly STD for BDS satellite DCBs

	BDS-only (ns)	BDS+GPS (ns)	DLR (ns)	CAS (ns)
GEO	0.218	0.198	0.173	0.099
IGSO	0.123	0.091	0.070	0.084
MEO	0.147	0.097	0.147	0.142

**Fig. 8** Time series of FY-3D receiver DCB for BDS

are 4.230 ± 0.202 ns and 3.794 ± 0.130 ns, respectively. There is an obvious deviation of 0.436 ns between monthly means of BDS-only and BDS+GPS solutions, which is much larger than the difference of 0.037 ns between GPS-only and BDS+GPS solutions. This is reasonable because the strength of BDS-only solution is relatively weak due to the few BDS onboard observations from FY-3D, and the fusion of BDS and GPS observation can significantly improve the solution strength. Moreover, the stability of BDS receiver DCB can be improved by 36% when using BDS+GPS solution. Note that there is also a periodic variation of about 6 days in the FY-3D receiver DCB for BDS, which is consistent with that of GPS. A possible reason has been discussed before.

Since VTEC and receiver DCB are highly correlated, the changes of plasmaspheric properties can affect the estimation of receiver DCB. Generally, such changes are caused by the variations of geomagnetism and solar activity. Figure 9 shows the Disturbed Storm Time (DST) and F10.7 in the period of interest, which reflects geomagnetic and solar activity conditions, respectively. Note that the receiver DCB of GPS for BDS+GPS solution is plotted together with the DST for the convenience of analysis. The DST and F10.7 indexes are available at <http://isgi.unistra.fr> and <ftp://ftp.ngdc.noaa.gov>, respectively. As shown in Fig. 9, the DST indexes during these days are larger than -30 nT. No obvious magnetic storms could be seen. Also, it can be found that the variations of DST index have little relationship with the variations of FY-3D receiver DCB. The F10.7 index varies between 66 and 74 sfu, which means quiet solar activity for the entire period of study. Note that the F10.7 index fluctuates a lot between

**Fig. 9** Time series of DST (top) and F10.7 (bottom) indexes of 29 days

DOY 359 and 360, but this fluctuation is not found in the receiver DCB during the 2 days. Therefore, it seems that neither DST index nor F10.7 index can explain the variations of GPS and BDS receiver DCBs.

As indicated in Yue et al. (2011), the variations of onboard receiver DCB may be affected by the receiver temperature. But Wautelet et al. (2017) analyzed the relationship between Jason-2 receiver DCB and the temperature obtained from the GPSP-B receiver onboard Jason-2 and found there was little correlation between them. Since we cannot obtain the temperature data of FY-3D receiver, the relationship between the onboard FY-3D receiver DCB and the FY-3D receiver temperature cannot be analyzed. The specific reason for the variation of FY-3D receiver DCB needs to be further investigated.

Based on the above analyses of BDS and GPS DCBs results of FY-3D, the monthly stability of satellite and receiver DCBs for BDS+GPS solutions can be improved compared with BDS-only and GPS-only solutions. The stability improvement can be attributed to higher number of onboard observations used in BDS+GPS solution, which can improve the solution strength of DCB estimation. Furthermore, the stability improvement for BDS satellite DCB is larger than that for GPS satellite DCB. It can be concluded that using BDS+GPS onboard observations to estimate

BDS and GPS DCBs is better than using BDS-only and GPS-only onboard observations from FY-3D.

Comparison with DCB estimation between FY-3D and FY-3C

Here, FY-3C onboard observations during the period from DOY 356, 2017 to DOY 019, 2018 are applied to estimate the BDS and GPS DCBs. The DCB results are compared with that of the FY-3D solutions. It should be mentioned that the BDS data of FY-3C in DOY 361-362, 2017, and DOY 002 and 008, 2018 are too short, so the BDS data of FY-3C during these days will not be used to estimate BDS DCB. But the BDS data can be used to make contributions to the estimation of GPS DCB for the BDS + GPS solution. Because the FY-3C cannot receive signal of BDS C13 satellite, the C13 satellite is excluded when making a comparison between FY-3D and FY-3C solutions.

The means of absolute difference for satellite DCB between onboard solutions and DCB products are shown in Table 2. For BDS satellites, the means of absolute difference for FY-3D solutions are obviously smaller than that for FY-3C solutions. This indicates that the monthly means of FY-3D solutions are much closer to DCB products compared with that of FY-3C solutions. For GPS satellites, the means of absolute difference for FY-3D solutions are slightly larger than that for FY-3C solutions with a difference smaller than 0.02 ns.

The mean values of monthly STD for BDS and GPS satellite DCBs are given in Table 3. For BDS satellites, the means of monthly STD for FY-3D solutions are much smaller than that of FY-3C solutions. Compared with FY-3C solutions, the stability for BDS GEO, IGSO and MEO satellites can be improved by (48%, 62%, 56%) for FY-3D BDS-only solution and (46%, 60%, 54%) for FY-3D BDS + GPS solution,

Table 2 Statistics of mean values of absolute difference for satellite DCB between onboard solutions and DCB products

Solution	LEO satellite	Mean of absolute difference (ns)	
		DLR	CAS
BDS			
BDS-only	FY-3D	0.434	0.502
	FY-3C	0.553	0.617
BDS + GPS	FY-3D	0.401	0.461
	FY-3C	0.538	0.549
GPS			
GPS-only	FY-3D	0.321	0.321
	FY-3C	0.310	0.313
BDS + GPS	FY-3D	0.322	0.323
	FY-3C	0.303	0.305

Table 3 Statistics of mean values of monthly STD for BDS and GPS satellite DCBs. The results of DLR and CAS products are shown as references

Solution	LEO Satellite	Mean of monthly STD (ns)			
		GPS	GEO	IGSO	MEO
BDS					
BDS-only	FY-3D	-	0.214	0.116	0.158
	FY-3C	-	0.408	0.305	0.361
BDS + GPS	FY-3D	-	0.194	0.096	0.106
	FY-3C	-	0.358	0.239	0.231
GPS					
GPS-only	FY-3D	0.098	-	-	-
	FY-3C	0.146	-	-	-
BDS + GPS	FY-3D	0.092	-	-	-
	FY-3C	0.142	-	-	-
DLR	-	0.050	0.171	0.066	0.154
CAS	-	0.044	0.099	0.085	0.144

respectively. For GPS satellites, the means of monthly STD for FY-3D solutions are also smaller than that of FY-3C solutions with a stability improvement of about 33% for both GPS-only and BDS + GPS solutions. It is worth noting that the means of monthly STD for BDS and GPS satellites when using onboard observations from FY-3C are worse than that shown by Li et al. (2017b). There may be two possible reasons for this phenomenon: (1) Li et al. (2017b) used data of 1-second interval in 2015 which can provide more useful observations for the DCB estimation. (2) The FY-3C GNOS suffers from receiver aging, which may affect the data quality of FY-3C onboard observations. In addition, the BDS and GPS results of FY-3C also show the BDS + GPS solution can improve the stability of BDS and GPS satellite DCBs compared with BDS-only and GPS-only solutions.

The performance of BDS and GPS receiver DCBs is shown in Table 4. For both BDS and GPS results, the STDs

Table 4 Statistics of monthly mean and STD of BDS and GPS receiver DCBs

Solution	LEO satellite	Mean (ns)	Std (ns)
BDS			
BDS-only	FY-3D	6.525	0.215
	FY-3C	9.219	0.512
BDS + GPS	FY-3D	6.056	0.128
	FY-3C	8.831	0.222
GPS			
GPS-only	FY-3D	-17.637	0.167
	FY-3C	-49.999	0.218
BDS + GPS	FY-3D	-17.600	0.131
	FY-3C	-49.926	0.200

of FY-3C receiver DCB are larger than that of FY-3D, which indicates the FY-3D receiver DCB has better stability. Compared with the FY-3C receiver DCB, the stability of the FY-3D receiver DCB is 58%, 42%, 23% and 35% higher for BDS-only, BDS + GPS (BDS result), GPS-only and BDS + GPS (GPS result) solutions, respectively. It is remarkable that there is an obvious difference between the monthly mean of BDS-only and BDS + GPS solutions for FY-3C, which has also happened in FY-3D; the possible reason has been introduced before. Furthermore, the stability of BDS + GPS solution for FY-3C can achieve better performance compared to that of BDS-only solution for FY-3C.

By the above comparisons of BDS and GPS DCB results between FY-3D and FY-3C in different solutions, it can be learned that the DCB results based on FY-3D onboard observations can achieve better performance compared with that based on FY-3C onboard observations. This can be attributed to the better data quality and more observations provided by the FY-3D GNOS instrument. Furthermore, the improvement of BDS results is more significant than that of GPS results. The DCB results of FY-3C in different solutions also provide another case to show that using BDS + GPS solution is better than using BDS-only and GPS-only solutions.

DCB estimation with FY-3D and FY-3C onboard observations

Here, the onboard BDS and GPS observations from both FY-3D and FY-3C are processed together to estimate the BDS and GPS DCBs, and only the BDS + GPS scheme is performed due to its better performance compared with BDS-only and GPS-only schemes. Because of the better performance of FY-3D GNOS compared with that of FY-3C GNOS, the DCB results of FY-3D + FY-3C solution will be compared with that of FY-3D-only solution.

Figure 10 shows the monthly mean differences of satellite DCB between onboard solutions and DCB products. For FY-3D and FY-3D + FY-3C solutions, their monthly mean differences with DCB products are within ± 1.0 and ± 1.5 ns. Compared with FY-3D solutions, the means of absolute difference with respect to DLR and CAS products are slightly reduced from 0.322 to 0.299 ns and from 0.323 to 0.303 ns for GPS satellites, respectively, when using FY-3D + FY-3C solution. However, the means of the absolute difference with respect to DLR and CAS products are slightly increased from 0.401 to 0.458 ns and from 0.461 to 0.499 ns for BDS satellites, respectively, when using FY-3D + FY-3C solution. The results of BDS and GPS DCBs are different.

Figure 11 shows the monthly STDs of GPS and BDS satellite DCBs. The mean values of monthly STD for GPS and BDS satellite DCBs are given in Table 5. For GPS satellites, the monthly STDs of GPS satellite DCB for FY-3D + FY-3C

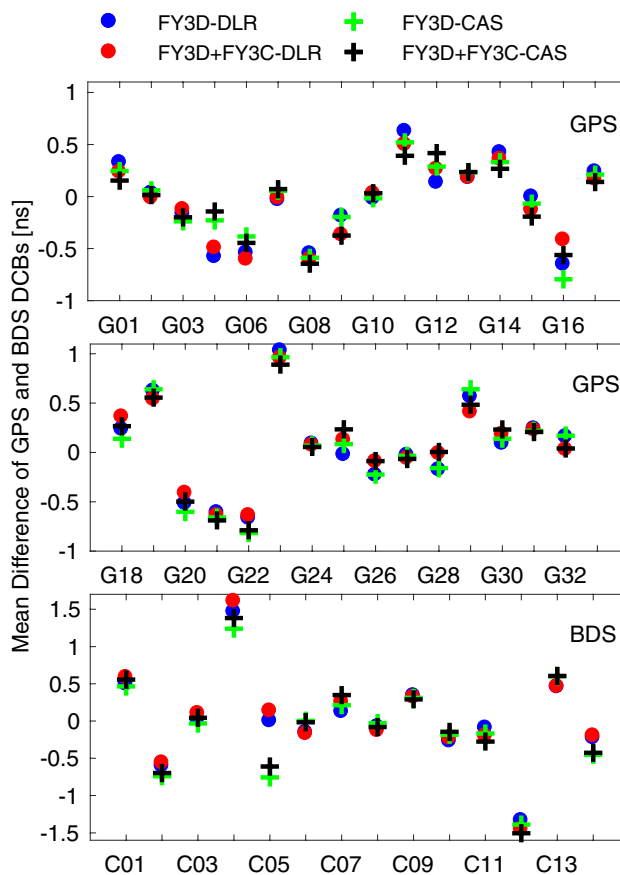


Fig. 10 Monthly mean differences of GPS (top, middle) and BDS (bottom) satellite DCBs between onboard solutions and DCB products

solution are generally smaller than that for FY-3D solution, and the GPS satellites DCBs can be improved by 16%. This stability improvement is reasonable, because the FY-3D + FY-3C solution can provide more observations which can improve the strength of DCB estimation. For BDS satellites, the situation is different from that of GPS. Compared with the FY-3D solution, the stability of BDS GEO and IGSO satellites DCBs for FY-3D + FY-3C solution can be improved by 9% and 7%, respectively, but the stability of BDS MEO satellite DCB is reduced by 8%. The reasons for the deterioration of MEO satellite DCB should be further investigated.

The time series of FY-3D receiver DCB is given in Fig. 12. For GPS and BDS results, the trends of time series for both FY-3D and FY-3D + FY-3C solutions are consistent with each other. As shown in Table 6, the differences between the monthly mean of FY-3D and FY-3D + FY-3C solutions are 0.011 and 0.027 ns for GPS and BDS receivers, respectively. Compared with the FY-3D solution, the FY-3D + FY-3C solution can improve the stability of 7% and 10% for receiver DCBs of GPS and BDS, respectively.

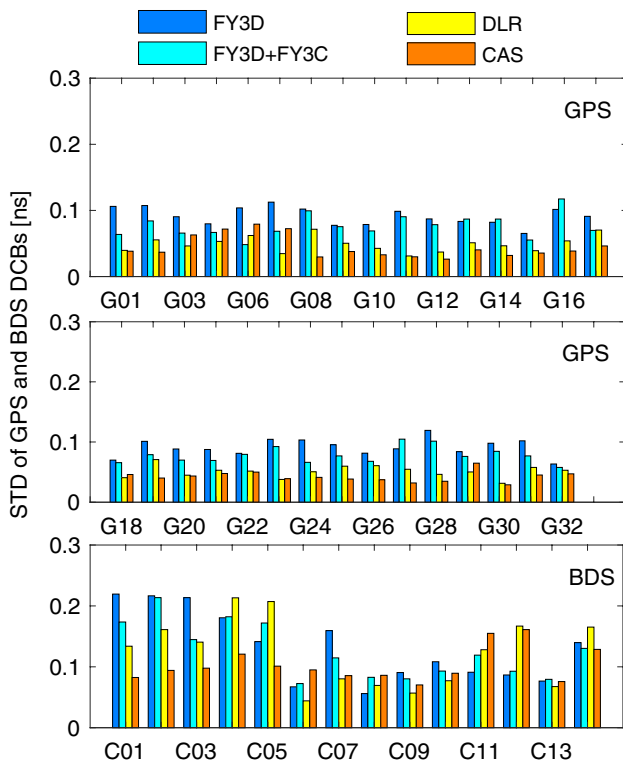


Fig. 11 Monthly STDs of GPS (top, middle) and BDS (bottom) satellite DCBs

Table 5 Statistics of mean values of monthly STD for GPS and BDS satellite DCBs

	FY-3D-only (ns)	FY-3D+FY-3C (ns)	DLR (ns)	CAS (ns)
GPS	0.092	0.077	0.050	0.044
GEO	0.194	0.177	0.171	0.099
IGSO	0.096	0.089	0.066	0.085
MEO	0.106	0.114	0.154	0.144

Though more onboard BDS and GPS observations can be provided by FY-3D + FY-3C solution compared with FY-3D-only solution which can improve the solution strength of DCB estimation, the results of BDS and GPS satellites DCBs are quite different. For GPS satellites, the DCB results of FY-3D + FY-3C solution has a better consistency with DLR and CAS products compared with that of FY-3D-only solution. For BDS satellites, the stability of GEO and IGSO satellites DCBs for FY-3D + FY-3C solution can be improved, but the stability of MEO satellite DCB is reduced. The reasons should be further investigated.

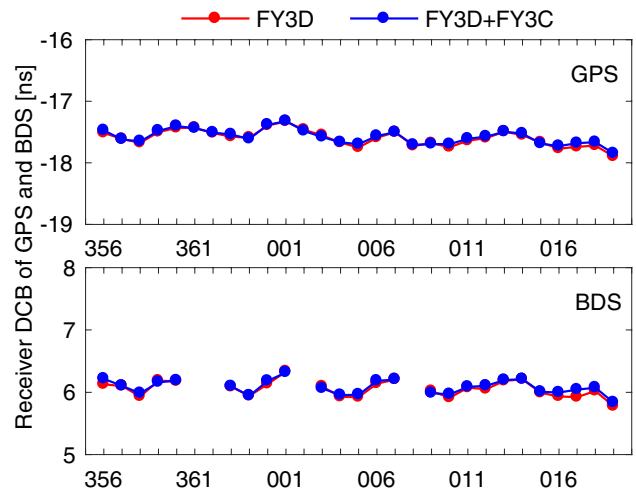


Fig. 12 Time series of FY-3D receiver DCB for GPS (top) and BDS (bottom)

Table 6 Statistics of monthly means and STDs of BDS and GPS receiver DCBs

	FY3D-only	FY3D + FY3C
MEAN(GPS) (ns)	-17.600	-17.589
STD(GPS) (ns)	0.131	0.122
MEAN(BDS) (ns)	6.056	6.083
STD(BDS) (ns)	0.128	0.115

Impact of DCB estimation on TEC estimation

Using the methodology introduced above, the VTEC along the LEO satellites orbit can be estimated with DCB simultaneously. Here, the VTECs of FY-3D based on three solutions, namely GPS-only, BDS + GPS and FY-3D + FY3C (using BDS + GPS scheme) are presented to discuss the impact of DCB estimation on TEC estimation.

The time series of the VTECs based on the three FY-3D solutions on the DOY 017, 2018 is illustrated in Fig. 13. In general, all the VTECs of the three solutions share similar variation trends and their amplitudes are about 6 TECU. The VTECs in Antarctica are generally larger than those in the Arctic. This is reasonable because the selected period is in the summer of the southern hemisphere, when the plasmasphere of southern hemisphere is more strongly ionized by solar radiation than that of northern hemisphere. In addition, the VTEC of the BDS + GPS solution is generally between the values of GPS-only and FY-3D + FY-3C solutions. It should be noted that there are negative values of estimated VTEC at high latitude for all three solutions, which has no physical meaning and may be due to the underestimation of DCB parameters (Wautelet et al. 2017; Li et al. 2017b). The ratio of the negative VTEC to all VTEC

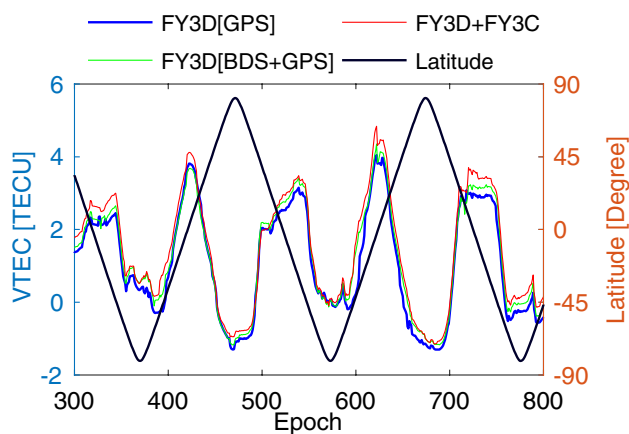


Fig. 13 Time series of the VTECs based on different FY-3D solutions and the corresponding latitude of the FY-3D orbit on the DOY 017, 2018

of GPS-only, BDS + GPS and FY-3D + FY3C solutions in 29 days are 28.21%, 26.24% and 25.55%, respectively. For FY-3D + FY3C solution, the estimated VTEC can reach more realistic results than GPS-only and BDS + GPS solutions, which is consistent with that of DCB estimation.

Conclusions

BDS and GPS onboard observations from FY-3D and FY-3C satellites during the period from DOY 356, 2017 to DOY 019, 2018 are processed to estimate BDS C2I-C7I and GPS C1C-C2W DCBs. Compared with the BDS-only and GPS-only solutions, the stability of satellite and receiver DCBs for both BDS and GPS has better consistency with the DCB products when using BDS + GPS solution. For GPS DCB, the stability of GPS satellite and receiver DCBs for BDS + GPS solution can be improved by 6% and 21%, respectively. For BDS DCB, the stability of BDS GEO, IGSO and MEO satellite DCB for BDS + GPS solution can be improved by (9%, 26%, 34%), and the stability improvement of BDS receiver DCB for BDS + GPS solution can reach about 36%. Also, the relationship between the variations of receiver DCB and geomagnetism and solar activity is analyzed. The result shows there is little relationship between them. Since we cannot obtain the temperature data of FY-3D GNOS, the relationship between temperature and the variations of receiver DCB should be further investigated.

Differences of the monthly mean and STD between FY-3D and FY-3C solutions are also studied. For GPS satellites, the stability of satellite DCB for FY-3D solution is better than that for FY-3C solution and the stability improvement for FY-3D solution can reach about 33%. For BDS satellites, the satellite DCB for FY-3D solution has better

consistency with DCB products than that for FY-3C solution. Compared with FY-3C solution, the stability of BDS GEO, IGSO and MEO satellites DCBs can be improved by 48%, 62% and 56% for FY-3D solution, respectively. Additionally, the receiver DCB of FY-3D is more stable than that of FY-3C, and the STD of FY-3D receiver DCB is 35% and 42% smaller than that of FY-3C receiver DCB for GPS and BDS, respectively. These improvements of FY-3D can be attributed to the better data quality and more observations provided by FY-3D GNOS instrument.

Moreover, both FY-3D and FY-3C onboard observations are processed together to estimate BDS and GPS DCBs. The results of GPS and BDS satellites DCBs are different. For GPS satellites, the DCB results for FY-3D + FY-3C solution have better consistency with the DLR and CAS products compared with FY-3D-only solution. The reason for this is that more onboard GPS observations can be provided by the FY-3D + FY-3C solution compared with FY-3D-only solution. For BDS satellites, the stability of BDS GEO and IGSO satellites DCBs for FY-3D + FY-3C solution can be improved by 9% and 7%, respectively, but the stability of BDS MEO satellite DCB for FY-3D + FY-3C solution is reduced by 8%, which should be further investigated. In addition, the impact of DCB estimation on TEC estimation is also discussed. The estimated VTEC along the FY-3D orbit for FY-3D + FY-3C solution can reach a more realistic result compared with that of GPS-only and BDS + GPS solutions. With the launch of more LEO satellites, the onboard observations are expected to make more contributions to GNSS DCB estimation.

Acknowledgements We would like to acknowledge DLR and CAS for providing access to the multi-GNSS products of differential code biases (DCBs). We are very grateful to the reviewers for their helpful remarks for improving this paper. We also sincerely thank Wenjin Yang for her kind support. The numerical calculations in this paper have been done on the supercomputing system in the Supercomputing Center of Wuhan University. This research was funded by the National Natural Science Foundation of China (Grant No. 41774030), the Hubei Province Natural Science Foundation of China (Grant No. 2018CFA081), and the National Youth Thousand Talents Program.

References

- Bai W, Sun Y, Du Q, Yang G, Yang Z, Zhang P, Bi Y, Wang X, Cheng C, Han Y (2014) An introduction to the FY3 GNOS instrument and mountain-top tests. *Atmos Meas Tech* 7(6):1817–1823. <https://doi.org/10.5194/amt-7-1817-2014>
- Blewitt G (1990) An automatic editing algorithm for GPS data. *Geophys Res Lett* 17(3):199–202. <https://doi.org/10.1029/GL017i003p00199>
- Cai Y, Bai W, Wang X et al (2017) In-orbit performance of GNOS on-board FY3-C and the enhancements for FY3-D satellite. *Adv Space Res* 60(12):2812–2821. <https://doi.org/10.1016/j.asr.2017.05.001>

- Foelsche U, Kirchengast G (2002) A simple “geometric” mapping function for the hydrostatic delay at radio frequencies and assessment of its performance. *Geophys Res Lett* 29(10):1473. <https://doi.org/10.1029/2001GL013744>
- Hernandez-Pajares M, Juan JM, Sanz J (1999) New approaches in global ionospheric determination using ground GPS data. *J Atmos Sol Terr Phys* 61(16):1237–1247. [https://doi.org/10.1016/S1364-6826\(99\)00054-1](https://doi.org/10.1016/S1364-6826(99)00054-1)
- Li M, Li W, Shi C, Jiang K, Guo X, Dai X, Meng X, Yang Z, Yang G, Liao M (2017a) Precise orbit determination of the Fengyun-3C satellite using onboard GPS and BDS observations. *J Geodesy* 91(11):1313–1327. <https://doi.org/10.1007/s00190-017-1027-9>
- Li W, Li M, Shi C, Fang R, Zhao Q, Meng X, Yang G, Bai W (2017b) GPS and BeiDou differential code bias estimation using Fengyun-3C satellite onboard GNSS observations. *Remote Sens* 9(12):1239. <https://doi.org/10.3390/rs9121239>
- Li X, Li X, Yuan Y, Zhang K, Zhang X, Wickert J (2018a) Multi-GNSS phase delay estimation and PPP ambiguity resolution: GPS, BDS, GLONASS, Galileo. *J Geodesy* 92(6):579–608. <https://doi.org/10.1007/s00190-017-1081-3>
- Li X, Xie W, Huang J, Ma T, Zhang X, Yuan Y (2018b) Estimation and analysis of differential code biases for BDS3/BDS2 using iGMAS and MGEX observations. *J Geodesy*. <https://doi.org/10.1007/s00190-018-1170-y>
- Lin J, Yue X, Zhao S (2016) Estimation and analysis of GPS satellite DCB based on LEO observations. *GPS Solut* 20(2):251–258. <https://doi.org/10.1007/s10291-014-0433-1>
- Mannucci AJ, Wilson BD, Yuan DN, Ho CH, Lindqwister UJ, Runge TF (1998) A global mapping technique for GPS-derived ionospheric total electron content measurements. *Radio Sci* 33(3):565–582. <https://doi.org/10.1029/97RS02707>
- Montenbruck O, Kroes R (2003) In-flight performance analysis of the CHAMP BlackJack GPS receiver. *GPS Solut* 7(2):74–86. <https://doi.org/10.1007/s10291-003-0055-5>
- Montenbruck O, Rizos C, Weber R, Weber G, Neilan R, Hugentobler U (2013) Getting a grip on multi-GNSS—the international GNSS service MGEX campaign. *GPS World* 24(7):44–49
- Montenbruck O, Hauschild A, Steigenberger P (2014) Differential code bias estimation using Multi-GNSS observations and global ionosphere maps. *Navigation* 61(3):191–201. <https://doi.org/10.1002/navi.64>
- Sanz J, Juan JM, Rovira-Garcia A, González-Casado G (2017) GPS differential code biases determination: methodology and analysis. *GPS Solut* 21(4):1549–1561. <https://doi.org/10.1007/s10291-017-0634-5>
- Schaer S (1999) Mapping and predicting the earth’s ionosphere using the global positioning system. Ph.D. thesis. Astronomisches Institut, Universität Bern, Switzerland
- Wang N, Yuan Y, Li Z, Montenbruck O, Tan B (2016) Determination of differential code biases with multi-GNSS observations. *J Geodesy* 90(3):209–228. <https://doi.org/10.1007/s00190-015-0867-4>
- Wautelet G, Loyer S, Mercier F, Perosanz F (2017) Computation of GPS P1–P2 differential code biases with Jason-2. *GPS Solut* 21(4):1619–1631. <https://doi.org/10.1007/s10291-017-0638-1>
- Yang J, Zhang P, Lu N, Yang Z, Shi J, Dong C (2012) Improvements on global meteorological observations from the current Fengyun 3 satellites and beyond. *Int J Digit Earth* 5(3):251–265. <https://doi.org/10.1080/17538947.2012.658666>
- Yue X, Schreiner WS, Hunt DC, Rocken C, Kuo YH (2011) Quantitative evaluation of the low earth orbit satellite based slant total electron content determination. *Space Weather* 9(9):S09001. <https://doi.org/10.1029/2011SW000687>
- Zakharenkova I, Cherniak I (2015) How can GOCE and TerraSAR-X contribute to the topside ionosphere and plasmasphere research? *Space Weather* 13(5):271–285. <https://doi.org/10.1002/2015SW001162>

Zhong J, Lei J, Dou X, Yue X (2016a) Is the long-term variation of the estimated GPS differential code biases associated with ionospheric variability? *GPS Solut* 20(3):313–319. <https://doi.org/10.1007/s10291-015-0437-5>

Zhong J, Lei J, Dou X, Yue X (2016b) Assessment of vertical TEC mapping functions for space-based GNSS observations. *GPS Solut* 20(3):353–362. <https://doi.org/10.1007/s10291-015-0444-6>

Publisher’s Note Springer Nature remains neutral with regard to jurisdictional claims in published maps and institutional affiliations.



Xingxing Li is currently a professor at Wuhan University. He has completed his B.Sc. degree at the school of Geodesy and Geomatics in Wuhan University. He obtained his Ph.D. degree at the Department of Geodesy and Remote Sensing of the German Research Centre for Geosciences (GFZ). His current research mainly involves GNSS precise data processing and its application for geosciences.



Tengzhou Ma is currently a post-graduate student in Wuhan University. He received his bachelor’s degree from the School of Geography and Planning, Sun Yat-Sen University in 2017. His research currently focuses on the DCB estimation and the extraction of the ionospheric TEC based on the LEO satellites.



Weiliang Xie is currently a Ph.D. candidate at GFZ. He has completed his B.Sc. at the School of Earth Science and Environmental Engineering at Southwest Jiao Tong University. His area of research currently focuses on the ionospheric modeling and the estimation and characteristics of multi-GNSS differential code bias.



Keke Zhang is currently a Master candidate at Wuhan University. He has completed his B.Sc. at the School of Geodesy and Geomatics in Wuhan University in 2016. His area of research currently focuses on GNSS precise orbit determination.



Xiaodong Ren is currently a post-doctoral candidate at Wuhan University. He obtained his Master and Doctor degrees with distinction in Geodesy and Engineering Surveying at the School of Geodesy and Geomatics in Wuhan University in 2011 and 2017. His main research focuses on PPP-RTK and ionospheric modeling.



Jiaxin Huang is currently a post-graduate student in Wuhan University. He has completed his B.Sc. at the School of Geodesy and Geomatics in Wuhan University in 2017. His research currently focuses on PPP-RTK and ionospheric modeling.